

1 Deciphering Bacterial and Archaeal Transcriptional Dark Matter and

2 Its Architectural Complexity

3 John S. A. Mattick^{1,*}, Robin E. Bromley^{1,*}, Kaylee J. Watson^{1,*}, Ricky S. Adkins^{1,*}, Christopher I. Holt¹,
4 Jarrett F. Lebov¹, Benjamin C. Sparklin¹, Tyonna S. Tyson¹, David A. Rasko^{1,2,3,4}, and Julie C. Dunning
5 Hotopp^{1,2,5, **}

6 ¹ Institute for Genome Sciences, University of Maryland School of Medicine, Baltimore, MD 21201, USA

7 ² Department of Microbiology and Immunology, University of Maryland School of Medicine, Baltimore,
8 MD 21201, USA

9 ³ Center for Pathogen Research, University of Maryland School of Medicine, Baltimore, MD 21201, USA

10 ⁴ Department of Microbial Pathogenesis, University of Maryland School of Dentistry, Baltimore, MD
11 21201, USA

12 ⁵ Greenebaum Cancer Center, University of Maryland School of Medicine, Baltimore, MD 21201, USA

13 **Current affiliation:**

14 John S. A. Mattick, University of Maryland, College Park, MD, USA

15 Benjamin C. Sparklin, AstraZeneca, Gaithersburg, MD, USA

16 Jarrett F. Lebov, Personal Genome Diagnostics, Baltimore, MD, USA

17 Tyonna Tyson, Hampton University, 100 E. Queen St., Hampton, VA 23668

18

19 * John S. A. Mattick, Robin E. Bromley, Kaylee J. Watson, and Ricky S. Adkins contributed equally to this
20 manuscript. They are listed in the chronological order that they contributed to the project/manuscript.

21 ** Corresponding author, jdhotopp@som.umaryland.edu

22

23 Running Title: Bacterial Transcript Dark Matter

24

25 Keywords: transcriptomics, bacterial transcripts, archaeal transcripts, small RNAs, non-coding RNA
26 (ncRNA), direct RNA sequencing

27 **Abstract**

28 Transcripts are potential therapeutic targets, yet bacterial transcripts remain biological dark matter with
29 uncharacterized biodiversity. We developed and applied an algorithm to predict transcripts for
30 *Escherichia coli* K12 and E2348/69 strains (Bacteria:gamma-Proteobacteria) with newly generated ONT
31 direct RNA sequencing data while predicting transcripts for *Listeria monocytogenes* strains Scott A and
32 RO15 (Bacteria:Firmicute), *Pseudomonas aeruginosa* strains SG17M and NN2 strains (Bacteria:gamma-
33 Proteobacteria), and *Haloflexax volcanii* (Archaea:Halobacteria) using publicly available data. From >5
34 million *E. coli* K12 ONT direct RNA sequencing reads, 2,484 mRNAs are predicted and contain more than
35 half of the predicted *E. coli* proteins. While the number of predicted transcripts varied by strain based
36 on the amount of sequence data used for the predictions, across all strains examined, the average size
37 of the predicted mRNAs is 1.6-1.7 kbp while the median size of the predicted bacterial 5'- and 3'- UTRs
38 are 30-90 bp. Given the lack of bacterial and archaeal transcript annotation, most predictions are of
39 novel transcripts, but we also predicted many previously characterized mRNAs and ncRNAs, including
40 post-transcriptionally generated transcripts and small RNAs associated with pathogenesis in the *E. coli*
41 E2348/69 *LEE* pathogenicity islands. We predicted small transcripts in the 100-200 bp range as well as
42 >10 kbp transcripts for all strains, with the longest transcript for two of the seven strains being the *nuo*
43 operon transcript, and for another two strains it was a phage/prophage transcript. This quick, easy,
44 inexpensive, and reproducible method will facilitate the presentation of operons, transcripts, and UTR
45 predictions alongside CDS and protein predictions in bacterial genome annotation as important
46 resources for the research community.

47 **Importance**

48 Our understanding of bacterial and archaeal genes and genomes is largely focused on proteins since
49 there have only been limited efforts to describe the bacterial/archaeal RNA diversity. This contrasts with

50 studies on the human genome, where transcripts were sequenced first through large scale EST
51 sequencing projects that preceded the release of the human genome over two decades ago. We
52 developed an algorithm for the quick, easy, inexpensive, and reproducible prediction of bacterial and
53 archaeal transcripts from ONT direct RNA sequencing data. These predictions are urgently needed for
54 more accurate studies examining bacterial/archaeal gene regulation, including regulation of virulence
55 factors, and for the development of novel RNA-based therapeutics and diagnostics to combat bacterial
56 pathogens, like those with extreme antimicrobial resistance.

57 Introduction

58 Genomics, genome-enabled technologies, computational biology, and large-scale data mining are
59 essential for rigorous, modern experiments on all organisms. Whole genome sequencing and protein-
60 based annotation are now routine, low-cost approaches for analyzing bacteria and archaea. But often
61 the annotation, and thus analysis and experimental validation, is limited to predicted protein-coding
62 regions and a few highly conserved non-coding RNAs (ncRNAs) like the rRNAs. Yet, pathogen RNA
63 transcripts, particularly ncRNAs and RNA-mediated regulation, offer an unexplored set of druggable
64 targets, diagnostics, and potential therapeutics (1). In this context, a transcript is a physical RNA
65 molecule that can be detected by sequencing RNA that has discrete start and end sites generated by a
66 diversity of molecular mechanisms (e.g., promoter/terminator, post-transcriptional processing).

67 Transcripts are encoded within operons but are distinct from operons, which also include regulatory
68 regions. Operons are widespread in bacterial/archaeal genomes, with ~630-700 operons in *Escherichia*
69 *coli* (2). Experimentalists have predicted operons using FPKM and/or sequencing depth without
70 algorithms (e.g. (3, 4)), and efforts have been made to develop algorithms for their prediction (5-11). For
71 example, the most recent version of Rockhopper predicts operons using a naïve Bayes classifier to
72 combine strand, intergenic distance, and coordinated differential expression in a unified probabilistic
73 model (12). Most operon predictions rely on the decades-old paradigm of operons as put forth by Jacob
74 and Monod (13), which was summarized recently as “sets of contiguous and functionally related genes
75 cotranscribed from a single promoter up to a single terminator” (14), including the operator regulatory
76 region.

77 Fundamentally, the classical definition of operon is a DNA-based definition, defining a region in DNA
78 that extends beyond the RNA-based transcripts to include the promoter/operator and terminator.
79 Operons can have multiple transcripts due to post-transcriptional processing (15), alternate terminators

80 (e.g. attenuation) (8, 16, 17), and alternate transcriptional initiation sites (14). There is a need for both
81 DNA-based annotation of operons and RNA-based annotation of transcripts. Fundamentally, RNA-seq is
82 transcript quantification, therefore it should be measured at the RNA/transcript level. Rockhopper has
83 been used for differential expression of its predicted operons (9), but it yields different results than the
84 corresponding transcript-focused analysis (14).

85 Currently mostly bacterial/archaeal RNA-seq studies are conducted using coding sequence (CDS)
86 predictions. Even when issues with counting algorithms are mitigated for a CDS-focused analysis of
87 polycistronic transcripts (18), measurements of CDSs in polycistronic transcripts are dependent on one
88 another yet are treated as independent measurements with the statistics used to detect differential
89 expression. This results in errors in variance estimations in differential expression tools (19).

90 Comparisons of StringTie and Rockhopper have previously noted some of these issues, as well as the
91 need for long RNA sequence reads to resolve these problems (8).

92 *E. coli* K12 is a well-studied genome that has some transcript predictions (17, 20), anti-sense RNA
93 characterization (21), and transcriptional start site and terminator predictions (17, 22-25), all of which
94 are aggregated and manually curated in RegulonDB (26) and EcoCyc (27). But even for this well studied
95 organism, reference GFF files lack transcript annotations, and it can be difficult, if not impossible, to
96 ascertain and use transcript structures for a differential expression analysis. The current work done to
97 characterize transcripts and transcriptional regulation in *E. coli* (e.g., (26)), while laudable and necessary,
98 is not possible for more than a few microorganisms, yet there is immense bacterial biodiversity.

99 Therefore, we sought to develop a fast, simple, rigorous, and reproducible method for identifying
100 bacterial transcripts that can be widely applied and takes advantage of recent advances in RNA
101 sequencing, including PacBio IsoSeq and Oxford Nanopore Technologies (ONT) direct RNA Sequencing
102 (14, 28-30). Transcript predictions will enable differential expression analyses using transcripts such that
103 the analyses can be expanded to include non-coding RNAs (ncRNAs) and also use the latest transcript-

104 based differential expression analysis tools like Salmon (31) and Kallisto (32). Transcript predictions are
105 also needed to inform consequences of genetic knock-in and knock-out experiments (e.g., (33)), identify
106 regulatory sequences (e.g., (8, 16, 34)) and detect post-transcriptional processing (e.g., (15, 35)). Recent
107 studies (8, 28, 36) reveal a much more complex picture of bacterial transcripts with post-transcriptional
108 processing and potentially multiple promoters and terminators, including transcripts beginning or
109 ending in the middle of adjacent coding sequences due to the coding density (17).

110 In this study, we describe a quick, easy, inexpensive, and reproducible method for whole transcriptome
111 sequencing and annotation using ONT direct RNA sequencing. We directly test the methods on the *E.*
112 *coli* K12 and E2348/69 strains and then also apply the algorithm to existing public data for *Pseudomonas*
113 *aeruginosa* strains SG17M and NN2 (37), *Listeria monocytogenes* strains Scott A and RO15 (38), and
114 *Haloflexax volcanii* (39). Ultimately, we envision genomes where operons, transcripts, and UTRs are all
115 annotated alongside CDSs and proteins in GFF files.

116 **Results**

117 **ONT direct RNA sequencing of *E. coli* transcripts**

118 We generated ONT direct RNA sequencing data (**Figure 1**) from RNA isolated from *E. coli* K12 and the
119 pathogenic *E. coli* E2348/69 (40) grown at 37 °C with aeration in LB and DMEM media (**Table 1, Table**
120 **A1**), which are virulence gene inducing growth conditions (15, 41-44). *E. coli* K12 is a well-studied
121 genome including previous transcript predictions (17, 20), anti-sense RNA characterization (21), and
122 transcriptional start site and terminator predictions (17, 22-25), all of which are aggregated and
123 manually curated in RegulonDB (26) and EcoCyc (27). The inclusion of *E. coli* E2348/69 allows us to
124 interrogate operon predictions in a related but clinically-relevant Enteropathogenic *E. coli* (EPEC) strain
125 with plasmids (40) that has pathogenesis-associated operons, which have had fine scale analysis of
126 transcription (15, 44). We focused on using ONT direct RNA sequencing, where RNA is sequenced

127 directly in the pore (**Figure 1K**) to predict bacterial transcripts because it does not have template
128 switching (36). Additionally, ONT direct RNA sequencing data lack genomic DNA contamination since
129 sequenced RNA and DNA have markedly different signals with RNA advancing through the pore more
130 slowly and with a higher electrical current range than DNA (**Figure 1E**). This difference between RNA and
131 DNA is seen in every RNA read as the sequencing transitions from the DNA-based adaptor to the RNA,
132 but is used to eliminate DNA reads with high fidelity. Therefore, we are confident that every read we
133 analyze arose from a transcript, which is tremendously powerful when considering alternative
134 transcripts, anti-sense transcripts, and non-coding RNA (ncRNA) predictions.

135 **Predicted *E. coli* K12 transcripts**

136 Using the 5,266,309 ONT reads generated for *E. coli* K12 (**Table 1**), we predicted transcripts using an
137 algorithm we developed, which is described below. We identified 3,902 strand-specific contiguously
138 transcribed (CT) regions in the K12 genome with 1,055 that have >20 reads that we used for predictions
139 (**Table 1**). The 1,055 CT regions used for predictions are on average 4 kbp and include 521 regions on the
140 (+)-strand spanning 2.07 Mbp and 534 regions on the (-)-strand spanning 2.14 Mbp (**Table 1**). There are
141 3,618 predicted transcripts with 1,465 predicted transcripts on the (+)-strand and 2,153 predicted
142 transcripts on the (-)-strand (**Table 1**). There are 289 (27%) regions with only a single transcript
143 predicted (**Table 1**), meaning the majority of CT regions contain more than one transcript either because
144 operons overlap or because there are multiple overlapping transcripts.

145 Of the 3,618 predicted transcripts, 2,484 are predicted to be mRNAs and 1,134 are predicted to be
146 ncRNAs (**Table 1**). mRNAs were defined as transcripts that have at least one annotated CDS found
147 completely within the transcript boundaries, whereas a ncRNA was defined as a transcript that lacks a
148 CDS found completely within the transcript boundaries. It is important to note that frequently the 5'-
149 end of CDSs (and the N-terminal portion of the protein encoded by them) are incorrectly annotated,

150 such that the assignment of transcripts as mRNA/ncRNA needs manual refinement in the future
151 including possible curation of the N-termini of proteins; additionally, protein annotation may be
152 informed and improved through transcript structural annotation. However, given these definitions, the
153 average mRNA was 1,618 bp with the smallest and largest being 131 bp and 13,305 bp, respectively
154 (**Table 1**). The average ncRNA was 517 bp with the smallest and largest being 52 bp and 2,947 bp,
155 respectively (**Table 1**). Of these 1,134 predicted ncRNAs, 23 (2%) were already described in the
156 reference GFF file and are ~23% of the 98 previously annotated ncRNAs in the reference GFF file (**Table**
157 **1**).

158 Of the 4,494 annotated coding sequences (CDSs), 2,357 were in an annotated transcript while 2,775
159 were not, suggesting that with these growth conditions we could annotate transcripts for approximately
160 half the CDSs. Of those, 1,341 (57%) CDSs were associated with a single transcript and 90% of CDSs were
161 associated with <4 transcripts (**Table 1, Figure 2A**). While 1,564 of the predicted transcripts contained
162 only a single CDS (**Table 1, Figure 2B**), the predicted transcript with the largest number of CDSs encoded
163 within it contained 17 CDSs, including *glf*, *gnd*, *insH7*, *rfbABCDX*, and *wbbHIJKL* (**Table 1**).

164 From the predicted mRNAs (excluding ncRNAs) and the predicted CDSs within those mRNAs, we
165 predicted the 5'- and 3'-untranslated regions (UTRs). The median 5'-UTR is 53 bp and the most common
166 length (mode) is 14 bp, while the median 3'-UTR has a median of 72 bp, and most common length
167 (mode) of 36 bp (**Table 1, Figure 2CD**). There are concerns that ONT sequencing cannot capture the
168 terminal 5'-end of transcripts. However, these results suggest that we are very close since it has been
169 previously shown that the 5'-UTR is 20-40 nt (24).

170 **Complexity of bacterial transcription**

171 Our predictions detect tremendous bacterial transcript structural variation while confirming previous
172 experimentally verified predictions. For example, in the *thr* operon, three transcripts are predicted,

173 including the previously described *thrL* transcript for the leader peptide, the *thrLABC* transcript, and a
174 *thrBC* transcript (45) (**Figure 1J**).

175 Other regions are more complex, like the region from 4,080-4,087 kbp encompassing *fdoGHI* and *fdhE*
176 (**Figure 3**). EcoCyc and RegulonDB describe this entire region as an operon with two promoters—one
177 that makes a transcript for the entire region and a second smaller internal transcript encoding *fdhE* that
178 is started from a promoter within *fdoH* (**Figure 3**). The ONT data suggest differential expression of the
179 transcript isoforms where *fdoGHI* are largely untranscribed in DMEM relative to LB while *fdhE* is
180 transcribed in both (**Figure 3**). A small ncRNA is observed in DMEM when *fdoG* is not transcribed. (**Figure**
181 **3**). Our algorithm predicts 11 different transcripts in this entire region, including the *fdhE* transcript that
182 starts in *fdoH* (**Figure 3**). As has been seen for decades in eukaryotic transcript prediction, automated
183 predictions require manual curation. The algorithm likely underpredicts long transcripts, due to the
184 limitations of the ONT technology as described below, so despite evidence for a complete *fdoGHI-fdhE*
185 transcript, we do not predict it, likely because there is insufficient depth (**Figure 3**). But there is robust
186 evidence for many of the other transcripts predicted that are not currently in RegulonDB, EcoCyc or the
187 GFF file, including a transcript of just *fdoG*, just *fdoGHI*, two putative overlapping small RNAs that
188 overlap the end of *fdoI* and the beginning of the *fdhE* transcript, and four putative overlapping small
189 RNAs that overlap the beginning of *fdoG* (**Figure 3**). In a typical differential expression analysis that uses
190 CDS regions., these four putative small RNAs overlapping *fdoG* would likely be misinterpreted as
191 expression of *fdoG* in DMEM. Importantly, while we detect these transcripts, we cannot ascertain that
192 they have a function, and they could merely be stable degradation products of transcription. Regardless,
193 they are likely to confound and obfuscate differential expression analyses.

194 Across the 11 transcripts predicted in the *fdoGHI-fdhE* region, there is imprecision in transcript start and
195 end sites, as previously described (15, 24). This variability includes slightly longer transcripts that extend
196 beyond *fdhE* that are observed under both growth conditions and was reproducible across all

197 sequencing runs (**Figure 3**). This variability is seen in many regions, suggesting that transcription and
198 termination are flexible.

199 **Predicted *E. coli* E2348/69 transcripts**

200 The 60% fewer reads sequenced for *E. coli* E2348/69 relative to K12 led to fewer transcript predictions
201 (**Table 1**), particularly fewer ncRNA predictions, but otherwise the results are quite similar. The longest
202 predicted mRNA for E2348/69 is *nuoABCDEFGHIJKLMN*, a known operon (46, 47). Unlike the K12 strain,
203 the E2348/69 strain contains two plasmids (NZ_CP059841.1 and NZ_CP059842.2, respectively) and
204 mRNA and ncRNAs were predicted on both plasmids. Of the 405 predicted ncRNAs, 3 (1%) were already
205 described in 4 ncRNAs in the reference GFF. Additional known ncRNAs missing in the reference GFF file
206 were identified, including *glmY* and *glmZ*, both of which are important for regulation of the *LEE* operon
207 and thus virulence (44).

208 The transcription of *LEE* operons, which are found in the E2348/69 genome, has been extensively
209 studied. In *LEE4*, a promoter upstream of *sepL* produces a *sepL-espADB* transcript that is post-
210 transcriptionally cleaved with RNase E to generate an *espADB* transcript and a *sepL* transcript that is
211 then further endonucleolytically degraded (15) (**Figure 4**). A putative transcriptional terminator was
212 previously identified downstream of *espB* within *cesD2*, but it was hypothesized that there is
213 readthrough transcription of the terminator (15). The ONT sequencing data here provide evidence for
214 readthrough of the transcriptional terminator. Very few reads included both the *cesD2-vapB-escF* region
215 and *sepL*, which may be an indication that processing to remove *sepL* is more efficient on the longer
216 transcript that terminates after *espF*, although we can't rule out that the 6 kbp transcript of the whole
217 region was not predicted due to the size limitations of ONT direct RNA sequencing. Consistent with the
218 latter, the 4 kbp *sepL-espADB* transcript has been detected by Northern blots in multiple studies (15,
219 44), yet it is very infrequently detected here. Prior 5'- and 3'-RACE of LEE4 transcripts revealed variation

220 in transcript ends, which we also detect, with multiple reads supporting a longer transcript at the 5'-end
221 of *sepL*, which seems to be a frequent phenomenon across all transcripts. We also predict single CDS
222 transcripts that encode for *espA*, *espB*, and *espF*.

223 **Data re-use and transcripts in *Listeria monocytogenes*, *Pseudomonas aeruginosa*, and**
224 ***Haloferax volcanii***

225 Through data re-use, we also predicted transcripts using published ONT data for *P. aeruginosa* strains
226 SG17M and NN2 (37), *L. monocytogenes* strains Scott A and RO15 (38), and *H. volcanii* (39). All five of
227 these strains had fewer sequencing reads than we had for *E. coli*, leading to fewer predictions of
228 transcripts, including both mRNA and ncRNA (**Table 1**). Yet we were still able to predict 274-1103
229 transcripts across the five strains and those transcripts were similar to the *E. coli* data with respect to
230 mean/median/mode 3'-UTR lengths, proportion of single CDS transcripts, proportion of single transcript
231 CDSs, size distribution of mRNA, and size distribution of ncRNA (**Table 1**). The 5'-UTR predictions were
232 similar across the bacterial strains, but the archaeal reads frequently did not extend beyond the 5'-end
233 of the CDS (**Table 1**). For a monocistronic transcript, the mRNA is erroneously called a ncRNA, while for a
234 polycistronic transcript, a very long 5'-UTR is predicted resulting in an increased median (**Table 1**). It may
235 be the 5'-end predictions of the CDS are flawed due to calling the longest ORF, or it may be that the *H.*
236 *volcanni* UTRs are shorter than the bacterial 5'-UTRS and/or not well captured with the ONT technology.
237 Across all seven strains examined, the longest transcript varied, although two were phage transcripts
238 and two were *nuo* transcripts (**Table 1**). The inclusion of *L. monocytogenes* was an important test case
239 since it is a firmicute with leading strand transcription bias (48), which led to fewer and longer CT
240 regions, but did not prevent high quality transcript predictions. While there was ONT direct RNA data for
241 further species of gamma-Proteobacteria, we limited this analysis to just two species with two strains
242 each from this taxon. Overall, these results suggest that this simple sequencing method combined with

243 our algorithm can be applied widely to archaeal/bacterial genomes to enable rigorous and robust
244 transcript predictions.

245 **Differential expression analysis**

246 These transcript predictions can be used in a differential expression analysis using Salmon and EdgeR as
247 demonstrated with existing E2348/69 short read data from the SRA (PRJEB36845/E-MTAB-88804) and
248 the long read ONT data generated here (**Figure 5**). Even when analyzing the same Illumina data, there is
249 discordance between the TPM values calculated for transcripts and CDSs (**Figure 5GHI**). There is also
250 discordance when quantifying the ONT data, which might be attributed to many factors, which bears
251 further investigation but is beyond the scope of this manuscript. We have concerns about using ONT
252 reads for differential expression analysis since shorter transcripts are preferentially sequenced relative
253 to longer transcripts (**Figure 6F**, as described below). In addition, the larger numbers of Illumina reads
254 generated is beneficial in the calculation of TPMs and subsequent statistical analyses.

255 **Features and Limitations of ONT direct RNA sequencing of *E. coli* transcripts**

256 To develop rigorous methods and algorithms to predict these transcripts, we needed to understand the
257 characteristics of ONT direct RNA sequencing of bacterial transcripts, which we expect to differ from
258 sequencing of eukaryotic transcripts given the differing physical features and stability of prokaryotic and
259 eukaryotic RNA. Overall, operons >5 kbp are difficult to obtain in a single read (**Figure 6A**), but reads can
260 be sequenced that span most predicted operons as well as exceed the boundaries of an existing operon
261 prediction (**Figure 6AB**). While *E. coli* has known transcripts >10 kbp, we do not generate reads >9 kbp
262 (**Table 1**). This is, at least in part, likely due to the ONT technology since we observe that (a) this is
263 reproducible across multiple systems and RNA molecules we know must be full length, like rRNAs
264 (**Figure 6C**), (b) there is 5'-truncation of transcripts in 11.7 kbp full-length *in vitro* transcribed (IVT)
265 polyadenylated RNA (**Figure 6D**), and (c) there are many incomplete reads for the 1.4 kbp yeast

266 enolase 2 (ENO2) RNA calibration strand provided by ONT (**Figure 6E**). Sequenced transcripts are also 3'-
267 truncated (**Figures 1ABCD, 3AC, 4ABCD**), as previously described for ONT (28, 36, 37) and PacBio IsoSeq
268 (30) sequencing of bacterial transcripts, possibly from (a) random fragmentation of RNA, (b) RNA
269 degradation, and/or (c) incomplete transcription in a bacterial cell. Additionally, we found that shorter
270 transcripts are preferentially sequenced relative to longer transcripts (**Figure 6F**). This is despite
271 counts/RPKMs being reported as well correlated between Illumina cDNA-based sequencing, ONT cDNA-
272 based sequencing, and ONT direct RNA sequencing (49), as well as when nanopore direct RNA
273 sequencing CPMs are compared to the absolute concentration of a spike-in (50).

274 To address incomplete reads and preferential sequencing of shorter transcripts, we developed a method
275 that first predicts transcript start/stop sites in locations where there is an over-abundance of reads
276 starting and ending. Subsequently, the actual transcripts are defined by measuring the strength of the
277 connection between those start and stop sites using a model that supports the characteristics of
278 truncated transcripts where smaller transcripts are preferentially sequenced. In this way, we can predict
279 12-15 kbp mRNAs (**Table 1**), despite having a shorter max ONT read length (**Figure A1**).

280 One of the features of ONT direct RNA sequencing is the ability to use changes in electrical current to
281 detect RNA modifications including *N*6-methyladenosine (m⁶A), 5-methylcytosine (m⁵C), inosine,
282 pseudouridine, and many more (51). At a minimum, posttranscriptional modifications are expected in
283 bacterial tRNA and rRNA (52), but might also be present in mRNA and would lead to nonrandom
284 changes in sequencing depth and base calling errors (53, 54). To alleviate this issue, we use a depth
285 calculation computed assuming every base is equally present in a read using start/end positions of bed
286 files for mapped reads. This also enables predictions in the presence of errors in the reference or
287 sequence divergence from the reference (e.g. (55)).

288 Using only read end positions may also facilitate predictions of transcripts for one strain using data from
289 a different strain. However, given that we haven't ascertained how much transcript structural diversity
290 there is between strains, it may be ill-advised. For that reason, we did not, for example, use the SG17M
291 and NN2 data to make available predictions for the research community for the frequently used *P.*
292 *aeruginosa* PA01.

293 Chimeric RNA sequencing reads were detected in all samples, including chimeras between the ONT
294 ENO2 calibration strand and sample RNA (**Figure 1H**). A subset of these are *in silico* chimeric reads, with
295 a spike observed in the electrical current when analyzing the raw signal data, indicating an open pore
296 state that was missed by the MinKNOW software. Others lack this spike and could be either ligase-
297 mediated chimeras or *in silico*-mediated chimeras where the open pore state was too short to be
298 detected (**Figure A2**) (56). In our analysis, this was addressed by removing the clipped portions of
299 mapped reads. When mapping reads to a reference genome, portions of a mapped read that do not align
300 with the reference will be either “soft-clipped” or “hard-clipped.” A soft clipped read has a portion that
301 does not align to any other area of the reference (e.g. the ENO2 portion of an ENO2/mRNA chimeric
302 read), whereas a hard clipped read has two portions that align to different parts of the genome. For
303 soft- and hard-clipped reads we used the primary alignment, ignoring the clipped portion of the read.

304 **Transcript Prediction Algorithm**

305 We developed an algorithm to predict transcripts based on these characteristics and applied it as
306 described above. Each CT region is examined separately along with the reads completely contained
307 within that region. CT regions are initially defined through the bed input file and subsequently refined to
308 subdivide regions based on a minimum depth cut-off (default=2). Ultimately a region needs to have a
309 minimum number of reads fully contained within it to be considered (default=2). The change in depth of

310 the sequencing reads for each genomic position of the CT region (D_{reg}) ignoring mismatches/indels is
311 calculated as

312
$$\Delta D_{\text{reg}} = D_{\text{reg}(n+1)} - D_{\text{reg}(n)}$$

313 Potential start and stop sites are predicted at positions where ΔD_{reg} is sufficiently positive/negative and
314 always includes the first and last position of the region. These predictions require that $|\Delta D_{\text{reg}}|$ surpasses
315 a threshold (default=4). ONT sequencing has issues identifying precise ends of transcripts due to polyA-
316 trimming as well as sequencing 5'-ends, such that predicted start/stop sites in close proximity
317 (default=100) are grouped.

318 Candidate transcripts are predicted using the Cartesian product of all predicted start and stop sites. The
319 total read count (N_{tot}) is calculated from the number of total reads that are mapped to all transcripts
320 that fully contains them, allowing for mapping to multiple transcripts. The count of exclusively assigned
321 reads (N_{ea}) is calculated after mapping each read to the shortest transcript that fully contains it. The
322 candidate transcripts are processed from shortest to longest computed as $\text{Ratio} = N_{\text{ea}} / N_{\text{tot}}$. If this ratio
323 is less than the threshold (default=0.2), the candidate transcript is discarded. If possible, reads from
324 discarded transcripts are re-assigned to longer transcripts, and the N_{ea} is recalculated such that reads
325 initially assigned to now discarded transcripts can be used to support a longer transcript. All transcripts
326 that meet the ratio at the end of the analysis are reported in a gff file and a bed file.

327 **Assembling ONT RNA reads**

328 We attempted to assemble the ONT direct RNA reads with existing tools, including TAMA
329 (tc_version_date_2020_12_14) (57), Cupcake (v.29.0.0) (58), and StringTie (v1.3.4d) (59). None of the
330 existing tools recapitulated the complexity of the bacterial transcripts accurately, leading us to develop a
331 new algorithm for the prediction of bacterial transcripts (**Figure A3**).

332 **Discussion**

333 In biology, dark matter is often used to describe functional portions of genomes that are not described
334 or annotated. In most bacteria, transcripts are largely dark matter, with CDSs often serving as a proxy,
335 albeit a poor one. Here, we show that bacterial long read transcriptome data can be used to predict
336 bacterial transcripts using a tool designed for the complexities and nuances of prokaryotic transcripts.
337 Application of this tool to ONT data from three organisms revealed extensive transcript structural
338 variation, transcription of RNA on both strands in some regions, overlapping transcripts, and a diversity
339 of non-coding RNAs. Fundamental biological differences such as a high coding density and polycistronic
340 transcripts in bacterial genetics lead to problems in applying transcript prediction tools developed for
341 the human genome. We cannot merely apply the same laboratory and computational methods that
342 were designed and optimized for humans and eukaryotic model organisms, with the false assumption
343 that they will work because bacteria are “simpler” than humans.
344 The transcript structural diversity highlights the need for algorithmic and analysis improvements that are
345 important for rigorous differential expression analyses, molecular evolution analyses, and other analyses
346 as well as laboratory experiments like making knock-outs/ins or promoter analysis. Coupling this with a
347 re-analysis of existing *E. coli* proteomics data would be enlightening and informative in understanding if
348 transcripts annotated as ncRNAs are producing previously undescribed proteins/peptides.
349 Yet, there is much room for improvement for bacterial transcript predictions, both through lab
350 experimentation and bioinformatics. We hope that attention to the recent developments in bacterial
351 transcript sequencing will lead to the development of more bioinformatics tools with a richness like that
352 seen for eukaryotic transcript prediction. The greatest improvement in the lab would be in obtaining
353 more full-length reads, particularly for long transcripts, which is a challenge for all long-read sequencing
354 platforms. For ONT, the new chemistry may improve the length, and further improvements may be
355 possible by altering the reverse transcription method needed to remove RNA secondary structure by
356 changing the enzyme (60).

357 The issue of missing the last few bases of the read, which represents the 5'-end of the transcript, is a
358 more significant issue for those looking for single base pair resolution of transcript ends. Ligating an
359 adaptor to the read prior to sequencing shows promise in addressing that issue (50, 61). However, these
360 are only likely to improve recovery of the 5'-ends of transcripts, but we saw a significant amount of
361 fragmentation at the 3'-ends that may be either incomplete transcription, 3'-degradation of transcripts,
362 random breakage, or sequencing biases that need to be better understood.

363 Incomplete transcription is intriguing and may reflect the fundamental biology since (a) bacterial
364 transcription and translation are coupled and (b) bacterial transcripts are short-lived and frequently in
365 the process of being synthesized, since bacterial mRNAs are made at a rate of 40-80 nt/sec (62) while
366 the average mRNA half-life is only 2-10 minutes (63). In contrast, eukaryotic RNAs have to be spliced to
367 create mature mRNA before being exported from the nucleus and have increased stability and a longer
368 half-life.

369 Some have noted the inaccuracy of ONT sequencing. There is the base inaccuracy, which should not
370 solely be considered inaccuracy. RNA is modified with over >160 different modifications (64), and much
371 of the inaccuracy is actually hyperaccuracy that is detecting those modifications but still trying to make
372 assignment in four base space. It is actually the notion that RNA sequence is in four base space that is
373 issue. That will improve as people develop base callers that expand beyond just four base space. We
374 avoid base “inaccuracy” by using only the read mapping coordinates.

375 When discussing taxonomy, Stephen J. Gould emphasized that “classifications both reflect and direct
376 our thinking” (65). Going on to say that “the way we order represents the way we think” (65).
377 Annotation has many similarities to taxonomy, and similarly genome annotation both reflects and
378 directs our thinking. For bacteria, annotation is protein-centric, influencing our results and ways of
379 thinking. Historically, this is likely due to the connection between the definition of a gene and protein,

380 but practically it also relates to the ease with which we can computationally predict proteins. However,
381 with new experimental methods and abilities, it is time for a sea change in bacterial genome annotation.
382 The experimental and computational methods here are inexpensive, easy, and quick, and thus they
383 should be implemented widely. Additionally, there is a need for associated new ontology standards for
384 describing transcripts and operons in annotation files that will better describe these features, similar to
385 changes made in eukaryotic annotation files to accommodate alternative splicing and alternative
386 transcripts (66). A harmonization of the two would be ideal, such that there is a standard that spans the
387 incredible biological diversity and commonalities across the domains of life.

388 **Conclusions**

389 Here we use bacterial long read transcriptome data and a new algorithm we developed to predict
390 transcripts from this data for two strains of three diverse bacterial species including both Gram-negative
391 and Gram-positive bacteria. Our analysis reveals a tremendous amount of transcript structural variation,
392 transcription of RNA on both strands in some regions, overlapping transcripts, and a diversity of non-
393 coding RNAs, which we provide as new annotation for these genomes. Bacterial transcriptional
394 structural variation has a richness that rivals or surpasses what is seen in eukaryotes and provides a rich
395 new set of therapeutic and diagnostic targets.

396 **Methods**

397 **Bacterial cultures**

398 Cryogenically preserved *E. coli* K12 MG1655 or E2348/69 were streaked onto an LB agar plate and
399 placed in an incubator overnight at 37 °C. A single colony was selected to inoculate LB broth for an
400 overnight culture. The overnight culture was diluted 1:100 in LB broth and harvested at the optical

401 density specified in **Table 1A**. For DMEM, overnight cultures were grown in LB broth and diluted 1:100 in
402 DMEM.

403 **RNA Isolation**

404 To isolate RNA, the Qiagen RNeasy Mini Kit was used according to Qiagen RNA Protect Reagent
405 Handbook Protocols 4 and 7 with Appendix B on-column DNase digestion (Qiagen, Hilden, Germany).
406 The RNA was assessed with UV-Vis spectrophotometry (Denovix DS-11, Wilmington, DE), Qubit RNA HS
407 Assay Kit (Fisher Scientific, Waltham, MA), and TapeStation RNA Screenshot (Agilent, Santa Clara, CA).
408 RNA preparations were stored at -80 °C until ready for polyadenylation and sequencing, except for the *E.*
409 *coli* K12 MG1655 harvested at an optical density OD₆₀₀ of 0.2. The RNA isolated from this one culture
410 was treated four different ways. For SRR27982843, 4 µg of the freshly isolated RNA was immediately
411 polyadenylated and then taken into library preparation and sequenced, as detailed below. The leftover
412 polyadenylated RNA was stored at -80 °C alongside the original RNA isolation which had been frozen
413 without polyadenylation. Two months later, the original, unpolyadenylated RNA was thawed and
414 polyadenylated just before library preparation and sequencing (SRR27982841). On that same day, the
415 RNA that had been polyadenylated before being frozen was thawed and taken directly into library
416 preparation and sequencing (SRR27982841). Four months after the original RNA isolation, the RNA that
417 had been polyadenylated before storing at -80 °C was thawed again and polyadenylated again before
418 library preparation and sequencing (SRR27982840).

419 **Oxford Nanopore Sequencing**

420 RNA was polyadenylated with *E. coli* poly(A) polymerase (M0276S, New England Biosciences, Ipswich,
421 Massachusetts) at 37 °C for 90 s – 30 min (Table S1) according to the manufacturer's protocol and
422 sequenced with the Direct RNA Sequencing kit (SQK-RNA002, Oxford Nanopore Sequencing, Oxford, UK)
423 according to protocol version DRS_9080_v2_revR_14Aug2019. The prepared RNA library was loaded

424 onto R9.4.1 flow cells (FLO-MIN106D) in a MinION device Mk1B (MIN-101B). Sequencing runs were
425 terminated at 24 h. Fast5 files were basecalled using Guppy version 6.4.2 generating FASTQ files with
426 the high accuracy model using the rna_r9.4.1_70bps_hac config file on a GPU cluster.

427 **Read Mapping, Transcript Prediction, and Analysis**

428 FASTQ files were mapped to the reference genome (**Table A2**) using minimap2 (v2.24-r1122)
429 (67)(options: -ax map-ont -t 2). Alignments were sorted and filtered with samtools (v1.11) (68) using
430 view (option: -F 2308) and generating bam files that were merged and indexed. BED files were
431 generated with bamToBed (v2.27.1) (69)(options: -s -c 6,4 -o distinct,count) and filtered with awk to
432 remove regions with fewer than 20 reads. The tp.py script was run in python (v.3.11.4). Statistics on
433 regions, predicted transcripts, and other features were calculated with perl (v5.30.2). Perl (v5.30.2) was
434 also used to merge the transcript and reference gff files and identify mRNAs, ncRNAs, and UTRs. ONT
435 sequencing, transcript predictions, and reference CDS predictions were visualized in R (v3.6.3). E2348/69
436 reads from the SRA for PRJEB36845/E-MTAB-88804 and counted against the E2348/69 with the
437 transcript predictions presented here using Salmon (v. 1.10.2) (31). Before differential expression was
438 assessed, genes not meeting the required CPM cutoff of 5 in at least 3 samples were removed. The
439 samples were grouped based on the treatment status, and differentially expressed genes were
440 identified with EdgeR v3.30.3 using the quasi-likelihood negative binomial generalized log-linear model.
441 Statistical significance was set at an FDR cutoff < 0.05 after correction with the Benjamini Hochberg
442 method. A heatmap was drawn in R v4.2.1 using heatmap.3 of the z-score transformed $\log_2(\text{TPM})$ values
443 for differentially expressed genes with the columns ordered based on a dendrogram generated using
444 pvclust v2.2-0.

445 The full set of commands are described at: <https://github.com/jdhotopp/tp.py-Direct-RNA-Sequencing->
446 Manuscript-/tree/main (a DOI will be acquired after commands are finalized following review of the
447 manuscript).

448 **Acknowledgements**

449 This project was funded by federal funds from the National Science Foundation grant number EF
450 2025384 and the National Institute of Allergy and Infectious Diseases, National Institutes of Health,
451 Department of Health and Human Services under grant numbers U19AI110820 and T32AI162579. The
452 funding body had no role in the design of the study and collection, analysis, and interpretation of data
453 and in writing the manuscript.

454 **Data availability**

455 The ONT FASTQ file accessions for the data generated in this proposal are SRR18061005, SRR18061002,
456 SRR27982845, SRR18061004, SRR18061003, SRR23886068, SRR27982844, SRR27982843, SRR27982842,
457 SRR27982841, and SRR27982840.

458 **References**

- 459 1. Eichner H, Karlsson J, Loh E. 2022. The emerging role of bacterial regulatory RNAs in
460 disease. *Trends Microbiol* 30:959-972.
- 461 2. Salgado H, Moreno-Hagelsieb G, Smith TF, Collado-Vides J. 2000. Operons in *Escherichia*
462 *coli*: genomic analyses and predictions. *Proc Natl Acad Sci U S A* 97:6652-7.
- 463 3. Mader U, Nicolas P, Depke M, Pane-Farre J, Debarbouille M, van der Kooi-Pol MM,
464 Guerin C, Derozier S, Hiron A, Jarmer H, Leduc A, Michalik S, Reilmann E, Schaffer M,
465 Schmidt F, Bessieres P, Noirot P, Hecker M, Msadek T, Volker U, van Dijl JM. 2016.
466 *Staphylococcus aureus* Transcriptome Architecture: From Laboratory to Infection-
467 Mimicking Conditions. *PLoS Genet* 12:e1005962.
- 468 4. Kroger C, MacKenzie KD, Alshabib EY, Kirzinger MWB, Suchan DM, Chao TC, Akulova V,
469 Miranda-CasoLuengo AA, Monzon VA, Conway T, Sivasankaran SK, Hinton JCD, Hokamp
470 K, Cameron ADS. 2018. The primary transcriptome, small RNAs and regulation of
471 antimicrobial resistance in *Acinetobacter baumannii* ATCC 17978. *Nucleic Acids Res*
472 46:9684-9698.
- 473 5. Bergman NH, Passalacqua KD, Hanna PC, Qin ZS. 2007. Operon prediction for sequenced
474 bacterial genomes without experimental information. *Appl Environ Microbiol* 73:846-54.
- 475 6. Pertea M, Ayanbule K, Smedinghoff M, Salzberg SL. 2009. OperonDB: a comprehensive
476 database of predicted operons in microbial genomes. *Nucleic Acids Res* 37:D479-82.
- 477 7. Taboada B, Estrada K, Ciria R, Merino E. 2018. Operon-mapper: a web server for precise
478 operon identification in bacterial and archaeal genomes. *Bioinformatics* 34:4118-4120.
- 479 8. Warrier I, Ram-Mohan N, Zhu Z, Hazery A, Echlin H, Rosch J, Meyer MM, van Opijnen T.
480 2018. The Transcriptional landscape of *Streptococcus pneumoniae* TIGR4 reveals a
481 complex operon architecture and abundant riboregulation critical for growth and
482 virulence. *PLoS Pathog* 14:e1007461.
- 483 9. McClure R, Balasubramanian D, Sun Y, Bobrovskyy M, Sumby P, Genco CA, Vanderpool
484 CK, Tjaden B. 2013. Computational analysis of bacterial RNA-Seq data. *Nucleic Acids Res*
485 41:e140.
- 486 10. Tjaden B. 2015. De novo assembly of bacterial transcriptomes from RNA-seq data.
487 *Genome Biol* 16:1.
- 488 11. Chen X, Chou WC, Ma Q, Xu Y. 2017. SeqTU: A Web Server for Identification of Bacterial
489 Transcription Units. *Sci Rep* 7:43925.
- 490 12. Tjaden B. 2020. A computational system for identifying operons based on RNA-seq data.
491 *Methods* 176:62-70.
- 492 13. Jacob F, Monod J. 1961. Genetic regulatory mechanisms in the synthesis of proteins. *J*
493 *Mol Biol* 3:318-56.

494 14. Forquet R, Jiang X, Nasser W, Hommais F, Reverchon S, Meyer S. 2022. Mapping the
495 Complex Transcriptional Landscape of the Phytopathogenic Bacterium *Dickeya dadantii*.
496 *mBio* 13:e0052422.

497 15. Lodato PB, Kaper JB. 2009. Post-transcriptional processing of the LEE4 operon in
498 enterohaemorrhagic *Escherichia coli*. *Mol Microbiol* 71:273-90.

499 16. Yanofsky C. 2007. RNA-based regulation of genes of tryptophan synthesis and
500 degradation, in bacteria. *RNA* 13:1141-54.

501 17. Adams PP, Baniulyte G, Esnault C, Chegireddy K, Singh N, Monge M, Dale RK, Storz G,
502 Wade JT. 2021. Regulatory roles of *Escherichia coli* 5' UTR and ORF-internal RNAs
503 detected by 3' end mapping. *Elife* 10.

504 18. Chung M, Adkins RS, Mattick JSA, Bradwell KR, Shetty AC, Sadzewicz L, Tallon LJ, Fraser
505 CM, Rasko DA, Mahurkar A, Dunning Hotopp JC. 2021. FADU: a Quantification Tool for
506 Prokaryotic Transcriptomic Analyses. *mSystems* 6.

507 19. Chung M, Bruno VM, Rasko DA, Cuomo CA, Munoz JF, Livny J, Shetty AC, Mahurkar A,
508 Dunning Hotopp JC. 2021. Best practices on the differential expression analysis of multi-
509 species RNA-seq. *Genome Biol* 22:121.

510 20. Karp PD, Ong WK, Paley S, Billington R, Caspi R, Fulcher C, Kothari A, Krummenacker M,
511 Latendresse M, Midford PE, Subhraveti P, Gama-Castro S, Muniz-Rascado L, Bonavides-
512 Martinez C, Santos-Zavaleta A, Mackie A, Collado-Vides J, Keseler IM, Paulsen I. 2018.
513 The EcoCyc Database. *EcoSal Plus* 8.

514 21. Lybecker M, Zimmermann B, Bilusic I, Tukhtubaeva N, Schroeder R. 2014. The double-
515 stranded transcriptome of *Escherichia coli*. *Proc Natl Acad Sci U S A* 111:3134-9.

516 22. Feng CQ, Zhang ZY, Zhu XJ, Lin Y, Chen W, Tang H, Lin H. 2019. iTerm-PseKNC: a
517 sequence-based tool for predicting bacterial transcriptional terminators. *Bioinformatics*
518 35:1469-1477.

519 23. Conway T, Creecy JP, Maddox SM, Grissom JE, Conkle TL, Shadid TM, Teramoto J, San
520 Miguel P, Shimada T, Ishihama A, Mori H, Wanner BL. 2014. Unprecedented high-
521 resolution view of bacterial operon architecture revealed by RNA sequencing. *mBio*
522 5:e01442-14.

523 24. Mendoza-Vargas A, Olvera L, Olvera M, Grande R, Vega-Alvarado L, Taboada B, Jimenez-
524 Jacinto V, Salgado H, Juarez K, Contreras-Moreira B, Huerta AM, Collado-Vides J, Morett
525 E. 2009. Genome-wide identification of transcription start sites, promoters and
526 transcription factor binding sites in *E. coli*. *PLoS One* 4:e7526.

527 25. Kim D, Hong JS, Qiu Y, Nagarajan H, Seo JH, Cho BK, Tsai SF, Palsson BO. 2012.
528 Comparative analysis of regulatory elements between *Escherichia coli* and *Klebsiella*
529 *pneumoniae* by genome-wide transcription start site profiling. *PLoS Genet* 8:e1002867.

530 26. Salgado H, Gama-Castro S, Lara P, Mejia-Almonte C, Alarcon-Carranza G, Lopez-Almazo
531 AG, Betancourt-Figueroa F, Pena-Loredo P, Alquicira-Hernandez S, Ledezma-Tejeida D,
532 Arizmendi-Zagal L, Mendez-Hernandez F, Diaz-Gomez AK, Ochoa-Praxedis E, Muniz-

533 Rascado LJ, Garcia-Sotelo JS, Flores-Gallegos FA, Gomez L, Bonavides-Martinez C, Del
534 Moral-Chavez VM, Hernandez-Alvarez AJ, Santos-Zavaleta A, Capella-Gutierrez S, Gelpi
535 JL, Collado-Vides J. 2023. RegulonDB v12.0: a comprehensive resource of transcriptional
536 regulation in *E. coli* K-12. *Nucleic Acids Res* doi:10.1093/nar/gkad1072.

537 27. Karp PD, Paley S, Caspi R, Kothari A, Krummenacker M, Midford PE, Moore LR,
538 Subhraveti P, Gama-Castro S, Tierrafría VH, Lara P, Muniz-Rascado L, Bonavides-
539 Martinez C, Santos-Zavaleta A, Mackie A, Sun G, Ahn-Horst TA, Choi H, Covert MW,
540 Collado-Vides J, Paulsen I. 2023. The EcoCyc Database (2023). EcoSal
541 Plus:eesp00022023.

542 28. Grünberger F, Knüppel R, Jüttner M, Fenk M, Borst A, Reichelt R, Hausner W, Soppa J,
543 Ferreira-Cerca S, Grohmann D. 2020. Exploring prokaryotic transcription, operon
544 structures, rRNA maturation and modifications using Nanopore-based native RNA
545 sequencing. *bioRxiv* doi:10.1101/2019.12.18.880849.

546 29. Pitt ME, Nguyen SH, Duarte TPS, Teng H, Blaskovich MAT, Cooper MA, Coin LJM. 2020.
547 Evaluating the genome and resistome of extensively drug-resistant *Klebsiella*
548 *pneumoniae* using native DNA and RNA Nanopore sequencing. *Gigascience* 9.

549 30. Yan B, Boitano M, Clark TA, Ettwiller L. 2018. SMRT-Cappable-seq reveals complex
550 operon variants in bacteria. *Nat Commun* 9:3676.

551 31. Patro R, Duggal G, Love MI, Irizarry RA, Kingsford C. 2017. Salmon provides fast and bias-
552 aware quantification of transcript expression. *Nat Methods* 14:417-419.

553 32. Bray NL, Pimentel H, Melsted P, Pachter L. 2016. Near-optimal probabilistic RNA-seq
554 quantification. *Nat Biotechnol* 34:525-7.

555 33. Mateus A, Shah M, Hevler J, Kurzawa N, Bobonis J, Typas A, Savitski MM. 2021.
556 Transcriptional and Post-Transcriptional Polar Effects in Bacterial Gene Deletion
557 Libraries. *mSystems* 6:e0081321.

558 34. Mejia-Almonte C, Busby SJW, Wade JT, van Helden J, Arkin AP, Stormo GD, Eilbeck K,
559 Palsson BO, Galagan JE, Collado-Vides J. 2020. Redefining fundamental concepts of
560 transcription initiation in bacteria. *Nat Rev Genet* 21:699-714.

561 35. Van Assche E, Van Puyvelde S, Vanderleyden J, Steenackers HP. 2015. RNA-binding
562 proteins involved in post-transcriptional regulation in bacteria. *Front Microbiol* 6:141.

563 36. Grunberger F, Ferreira-Cerca S, Grohmann D. 2022. Nanopore sequencing of RNA and
564 cDNA molecules in *Escherichia coli*. *RNA* 28:400-417.

565 37. Pust MM, Davenport CF, Wiehlmann L, Tummler B. 2022. Direct RNA Nanopore
566 Sequencing of *Pseudomonas aeruginosa* Clone C Transcriptomes. *J Bacteriol*
567 204:e0041821.

568 38. Duru IC, Ylinen A, Grigore-Gurgu L, Riedel CU, Paulin L, Auvinen P. 2022. RNA editing,
569 RNA modifications, and transcriptional units in *Listeria monocytogenes*, PREPRINT
570 (Version 1). doi:<https://doi.org/10.21203/rs.3.rs-1530110/v1>.

572 39. Grünberger F, Knüppel R, Jüttner M, Fenk M, Borst A, Reichelt R, Hausner W, Soppa J,
573 Ferreira-Cerca S, Grohmann D. 2019. Exploring prokaryotic transcription, operon
574 structures, rRNA maturation and modifications using Nanopore-based native RNA
575 sequencing. *bioRxiv* doi:doi.org/10.1101/2019.12.18.880849.

576 40. Iguchi A, Thomson NR, Ogura Y, Saunders D, Ooka T, Henderson IR, Harris D,
577 Asadulghani M, Kurokawa K, Dean P, Kenny B, Quail MA, Thurston S, Dougan G, Hayashi
578 T, Parkhill J, Frankel G. 2009. Complete genome sequence and comparative genome
579 analysis of enteropathogenic *Escherichia coli* O127:H6 strain E2348/69. *J Bacteriol*
580 191:347-54.

581 41. Hazen TH, Daugherty SC, Shetty AC, Nataro JP, Rasko DA. 2017. Transcriptional Variation
582 of Diverse Enteropathogenic *Escherichia coli* Isolates under Virulence-Inducing
583 Conditions. *mSystems* 2.

584 42. Hazen TH, Michalski J, Luo Q, Shetty AC, Daugherty SC, Fleckenstein JM, Rasko DA. 2017.
585 Comparative genomics and transcriptomics of *Escherichia coli* isolates carrying virulence
586 factors of both enteropathogenic and enterotoxigenic *E. coli*. *Sci Rep* 7:3513.

587 43. Hazen TH, Daugherty SC, Shetty A, Mahurkar AA, White O, Kaper JB, Rasko DA. 2015.
588 RNA-Seq analysis of isolate- and growth phase-specific differences in the global
589 transcriptomes of enteropathogenic *Escherichia coli* prototype isolates. *Front Microbiol*
590 6:569.

591 44. Gruber CC, Sperandio V. 2014. Posttranscriptional control of microbe-induced
592 rearrangement of host cell actin. *mBio* 5:e01025-13.

593 45. Cho BK, Zengler K, Qiu Y, Park YS, Knight EM, Barrett CL, Gao Y, Palsson BO. 2009. The
594 transcription unit architecture of the *Escherichia coli* genome. *Nat Biotechnol* 27:1043-9.

595 46. Archer CD, Elliott T. 1995. Transcriptional control of the *nuo* operon which encodes the
596 energy-conserving NADH dehydrogenase of *Salmonella typhimurium*. *J Bacteriol*
597 177:2335-42.

598 47. Leif H, Sled VD, Ohnishi T, Weiss H, Friedrich T. 1995. Isolation and characterization of
599 the proton-translocating NADH: ubiquinone oxidoreductase from *Escherichia coli*. *Eur J
600 Biochem* 230:538-48.

601 48. Glaser P, Frangeul L, Buchrieser C, Rusniok C, Amend A, Baquero F, Berche P, Bloecker H,
602 Brandt P, Chakraborty T, Charbit A, Chetouani F, Couve E, de Daruvar A, Dehoux P,
603 Domann E, Dominguez-Bernal G, Duchaude E, Durant L, Dussurget O, Entian KD, Fsihi H,
604 Garcia-del Portillo F, Garrido P, Gautier L, Goebel W, Gomez-Lopez N, Hain T, Hauf J,
605 Jackson D, Jones LM, Kaerst U, Kreft J, Kuhn M, Kunst F, Kurapkat G, Madueno E,
606 Maitournam A, Vicente JM, Ng E, Nedjari H, Nordsiek G, Novella S, de Pablos B, Perez-
607 Diaz JC, Purcell R, Remmel B, Rose M, Schlueter T, Simoes N, et al. 2001. Comparative
608 genomics of *Listeria* species. *Science* 294:849-52.

609 49. Garalde DR, Snell EA, Jachimowicz D, Sipos B, Lloyd JH, Bruce M, Pantic N, Admassu T,
610 James P, Warland A, Jordan M, Ciccone J, Serra S, Keenan J, Martin S, McNeill L, Wallace
611 EJ, Jayasinghe L, Wright C, Blasco J, Young S, Brocklebank D, Juul S, Clarke J, Heron AJ,

612 Turner DJ. 2018. Highly parallel direct RNA sequencing on an array of nanopores. *Nat*
613 Methods 15:201-206.

614 50. Parker MT, Knop K, Sherwood AV, Schurch NJ, Mackinnon K, Gould PD, Hall AJ, Barton
615 GJ, Simpson GG. 2020. Nanopore direct RNA sequencing maps the complexity of
616 Arabidopsis mRNA processing and m(6)A modification. *Elife* 9.

617 51. Furlan M, Delgado-Tejedor A, Mulroney L, Pelizzola M, Novoa EM, Leonardi T. 2021.
618 Computational methods for RNA modification detection from nanopore direct RNA
619 sequencing data. *RNA Biol* 18:31-40.

620 52. Anonymous. 2011. Ribosomes: Structure, Function, and Dynamics.
621 SpringerWienNewYork, Austria.

622 53. Liu H, Begik O, Lucas MC, Ramirez JM, Mason CE, Wiener D, Schwartz S, Mattick JS,
623 Smith MA, Novoa EM. 2019. Accurate detection of m(6)A RNA modifications in native
624 RNA sequences. *Nat Commun* 10:4079.

625 54. Piechotta M, Naarmann-de Vries IS, Wang Q, Altmuller J, Dieterich C. 2022. RNA
626 modification mapping with JACUSA2. *Genome Biol* 23:115.

627 55. Chandler CE, Horspool AM, Hill PJ, Wozniak DJ, Schertzer JW, Rasko DA, Ernst RK. 2019.
628 Genomic and Phenotypic Diversity among Ten Laboratory Isolates of *Pseudomonas*
629 aeruginosa PAO1. *J Bacteriol* 201.

630 56. White R, Pellefigues C, Ronchese F, Lamiable O, Eccles D. 2017. Investigation of chimeric
631 reads using the MinION. *F1000Res* 6:631.

632 57. Kuo RI, Cheng Y, Zhang R, Brown JWS, Smith J, Archibald AL, Burt DW. 2020. Illuminating
633 the dark side of the human transcriptome with long read transcript sequencing. *BMC*
634 Genomics 21:751.

635 58. Tseng E. 2023. cDNA_Cupcake. https://github.com/Magdolla/cDNA_Cupcake. Accessed
636 05/11/2023.

637 59. Shumate A, Wong B, Pertea G, Pertea M. 2022. Improved transcriptome assembly using
638 a hybrid of long and short reads with StringTie. *PLoS Comput Biol* 18:e1009730.

639 60. Zeglinski K, Montellese C, Ritchie ME, Alhamdoosh M, Vonarburg C, Bowden R, Jordi M,
640 Gouil Q, Aeschimann F, Hsu A. 2023. An optimised protocol for quality control of gene
641 therapy vectors using Nanopore direct RNA sequencing. *bioRxiv*
642 doi:<https://www.biorxiv.org/content/10.1101/2023.12.03.569756v1:2023.12.03.569756>
643 .

644 61. Yan B, Tzertzinis G, Schildkraut I, Ettwiller L. 2022. Comprehensive determination of
645 transcription start sites derived from all RNA polymerases using ReCappable-seq.
646 *Genome Res* 32:162-174.

647 62. (ed). 2015. *Cell Biology by the Numbers* (Draft July 2015). book.bionumbers.org.
648 Accessed May 22, 2022.

649 63. Laalami S, Zig L, Putzer H. 2014. Initiation of mRNA decay in bacteria. *Cell Mol Life Sci*
650 71:1799-828.

651 64. Hofer K, Jaschke A. 2018. Epitranscriptomics: RNA Modifications in Bacteria and
652 Archaea. *Microbiol Spectr* 6.

653 65. Gould SJ. 1983. *Hen's Teeth and Horse's Toes: Further Reflections in Natural History*. W.
654 W. Norton & Company.

655 66. Gerstein MB, Bruce C, Rozowsky JS, Zheng D, Du J, Korbel JO, Emanuelsson O, Zhang ZD,
656 Weissman S, Snyder M. 2007. What is a gene, post-ENCODE? History and updated
657 definition. *Genome Res* 17:669-81.

658 67. Li H. 2018. Minimap2: pairwise alignment for nucleotide sequences. *Bioinformatics*
659 34:3094-3100.

660 68. Li H, Handsaker B, Wysoker A, Fennell T, Ruan J, Homer N, Marth G, Abecasis G, Durbin
661 R. 2009. The Sequence Alignment/Map format and SAMtools. *Bioinformatics* 25:2078-9.

662 69. Quinlan AR. 2014. BEDTools: The Swiss-Army Tool for Genome Feature Analysis. *Curr
663 Protoc Bioinformatics* 47:11 12 1-34.

664

665 **Tables**

666 **Table 1. Characteristics of Predicted Transcripts for *Escherichia coli*, *Listeria monocytogenes*, and *Pseudomonas aeruginosa***

Feature	<i>Escherichia coli</i> K12 (GCF_000005845.2)	<i>Escherichia coli</i> E2348/69 (GCF_014117345.2)	<i>Listeria monocytogenes</i> Scott A (CM001159.1)	<i>Listeria monocytogenes</i> RO15 (CADEHJ000000000.1)	<i>Pseudomonas aeruginosa</i> SG17M (NZ_CP080369.1)	<i>Pseudomonas aeruginosa</i> NN2 (NZ_LT883143.1)	<i>Pseudomonas aeruginosa</i> NN2 (NZ_LT883143.1)	<i>Haloflexax volcanii</i> (GCF_00025685.1)
Number of contigs in reference	1	3	1	2	1	1	1	5
Number of reads used	5,266,309	3,025,047	1,679,073	1,664,744	220,553	1,196,279	1,196,279	1,438,670
Number of CT Regions for Predictions (>20 reads)	1,055	1,071	525	464	391	1,209	1,209	640
Number of Regions on (+)-strand	521	528	238	206	181	612	612	318
Number of Regions on the (-)-strand	534	543	287	258	210	597	597	322
Span (bp) on (+)-strand	2,068,709	1,951,551	703,660	589,005	530,329	1,944,294	1,944,294	893,429
Span (bp) on (-)-strand	2,135,707	1,827,581	821,637	759,698	589,348	1,886,100	1,886,100	974,115
Average span (bp) + strand	3,968	3,777	2,946	2,848	2,915	3,174	3,174	2,807
Average span (bp) - strand	3,997	3,446	2,851	2,932	2,786	3,155	3,155	3,022
Number of Transcripts	3,618	2248	881	793	274	1103	1103	613
Number of Transcripts on the (+)-strand	1,465	1101	402	361	79	495	495	241
Number of Transcripts on the (-)-strand	2,153	1147	479	432	195	608	608	372
Number of Regions with 1 transcript	289	429	218	199	85	258	258	226
Maximum Number of Transcripts per Region	254	141	32	31	68	63	63	27
Mean 3'-UTR (bp)	150	126	122	112	163	236	236	180
Median 3'-UTR (bp)	72	62	48	47	59	78	78	84
Maximum 3'-UTR (bp)	2,716	1,261	1,306	1,245	2,235	2,809	2,809	2,040
Mean 5'-UTR (bp)	134	119	137	114	185	205	205	373
Median 5'-UTR (bp)	53	49	36	33	93	85	85	207*
Maximum 5'-UTR (bp)	2,122	2,817	2,303	2,303	1,835	1,943	1,943	2,955
Number of genes	4,494	4,809	3,038	3,149	6,349	6,380	6,380	3,956
Number of genes in annotated transcript	2,360	2,037	765	680	209	765	765	385
Number of genes associated with just 1 transcript	1,341	1,300	636	554	168	572	572	301
Maximum number of transcripts a single gene is associated with	15	12	6	7	4	6	6	10
90% of genes are associated with fewer than this number transcripts	4	4	3	3	3	3	3	3
Number of transcripts with 1 gene	1,563	1,096	349	316	79	398	398	167
Maximum number of genes in a single mRNA	17	14	38	22	15	15	15	15
90% of transcripts have fewer than this many genes	4	4	4	3	3	3	3	3
Number of predicted mRNAs	2,487	1,844	536	491	133	601	601	263
Average predicted mRNA size (bp)	1,617	1,732	1,660	1,607	1,590	1,735	1,735	1,948
Largest predicted mRNA (bp)	13,305	15,256	29,034	10,791	14,168	12,709	12,709	10,463
Smallest predicted mRNA (bp)	131	129	224	209	183	146	146	136
Number of predicted ncRNAs (including ones in reference GFF)	1,131	404	345	302	141	502	502	350*
Average predicted ncRNA size (bp)	550	649	497	524	578	538	538	724*
Largest predicted ncRNA (bp)	2,947	2,916	2,585	2,588	6,361	2,851	2,851	3,045*
Smallest predicted ncRNA (bp)	89	80	95	136	97	77	77	81*
Genes in longest mRNA	glf, gnd, insH7, rfbABCDX, wbbHIJKL	nuoABCEFGHIJKLMNOP	phage (LMOSA_9400-LMOSA_9770)	rplBCDEFNOPRVWX, rpmCD, rpsCEHJQS, secY	fusA, rplJL, rpoBC, rpsGL, tuf	(PANN_06920 - PANN_07050)	nuoABCD1HIJ1J2KLMN	phage

*The reads for this species frequently do not extend beyond the 5'-end of the CDS, essentially meaning transcripts start where translation is predicted to start. When this happens for a polycistronic transcript, the result is a very long 5'-UTR as seen with the increased median, and when this happens for a monocistronic transcript, the mRNA is erroneously called a ncRNA. While this likely occurs for all of the organisms, it is acute for the *H. volcanii* data. It may be that the 5'-end predictions of the CDS are flawed due to calling the longest ORF, or it may be that the *H. volcanii* UTRs are shorter than the bacterial 5'-UTRs.

667
668
669
670
671

672 **Figures**

673 **Figure 1 – Overview of the Experimental/Analysis Workflow**

674 Plus-strand ONT direct RNA sequencing reads (shown as lines) are mapped from 1 bp to 6 kbp in the *E.*
675 *coli* K12 genome (NC_000913.3), which corresponds to the *thr* operon, and sorted by their transcription
676 stop site for *E. coli* K12 grown in rich LB media (left sorted, **A**; right sorted, **C**) and DMEM media (left
677 sorted, **B**; right sorted, **D**). Our algorithm predicts 3 transcripts (**E**), and 4 CDSs in the GFF file are
678 illustrated (**F**). The transcript for the leader peptide *thrL* is recovered in both growth conditions. (**G**) RNA
679 was isolated from *E. coli* K12 grown at 37 °C with aeration in LB and DMEM media. (**H**) Squiggle plot for
680 two sequencing reads in tandem. In this case, the open pore state was missed by the software resulting
681 in a chimeric read. In both reads the DNA adapter can be observed with lower current followed by a
682 relative flat plateau that corresponds to the polyA tail. This is followed by the current changes
683 associated with the RNA moving through the pore. (**I**) Squiggle plots are shown of current for the same
684 length DNA and RNA highlighting that the signal to base ratio is different for RNA and DNA. (**J**) The
685 standard ONT direct RNA sequencing library was used on bacterial RNA that was *in vitro* polyadenylated
686 following RNA isolation. Library construction and (**K**) loaded on an ONT MinION device for nanopore
687 sequencing.

688 **Figure 2 – Characteristics of Transcript Predictions**

689 The distribution of the number of instances of CDS by transcripts/CDS (**A**) and the distribution of the
690 number of instances of transcripts by CDSs/transcript (**B**) are shown for *E. coli* K12, *E. coli* E2368/69, *L.*
691 *monocytogenes* ScottA, *L. monocytogenes* RO15, *P. aeruginosa* SG17M, *P. aeruginosa* NN2, and *H.*
692 *volcanii*. The data points in these discrete distributions are connected by lines for visualization purposes.
693 The inset in each illustrates how transcripts/CDS and CDSs/transcript are defined. The size distributions

694 of predicted 5'-UTRs (**C**) and 3'-UTRs (**D**) are plotted for each of the six strains examined with an inset
695 that zooms in on 0-350 bp to better illustrate the distribution of the majority of the data.

696 **Figure 3 – *fdoGHI-fdhE* Transcripts**

697 Reads mapping to the minus strand of the *E. coli* K12 genome (NC_000913.3) grown in LB (**A, C**) and
698 DMEM (**B, D**) are shown for a region from 4,080-4,088 kbp. To facilitate the visualization of the starts
699 and stops of transcripts, reads were sorted by either their left most (**A, B**) or right most (**C, D**) position
700 and plotted from top to bottom accordingly. Transcript predictions from our algorithm (**E**) and the
701 predicted CDSs in the reference gff file (**F**) are shown with arrows indicating the direction of
702 transcription and with transcripts/CDSs on the different strands having different shading (light for the
703 (+)-strand and dark for the (-)-strand).

704 **Figure 4 – LEE4 Operon**

705 Reads are illustrated that map to the plus strand (**A, C**) and minus strand (**B, D**) of the *E. coli* E2348/69
706 genome (GCF_014117345.2) grown in LB or DMEM for a region from 72-78 kbp. There are no reads from
707 the LB conditions on the (+)-strands. To facilitate the visualization of the starts and stops of transcripts,
708 reads were sorted by either their left most (**A, B**) or right most (**C, D**) position and plotted from top to
709 bottom accordingly. Transcript predictions from our algorithm (**E**) and the predicted CDSs in the
710 reference gff file (**F**) are shown with arrows indicating the direction of transcription and with
711 transcripts/CDSs on the different strands having different shading (light for the (+)-strand and dark for
712 the (-)-strand).

713 **Figure 5 – Differential expression of predicted transcripts**

714 Reads are illustrated mapping to the plus strand of the *E. coli* E2348/69 genome (GCF_014117345.2)
715 grown in LB (**A, C**) or DMEM (**B, D**) from 4.730-4.735 Mbp sorted by either their left most (**A, B**) or right
716 most (**C, D**) position. Transcript predictions from our algorithm (**E**) and the predicted CDSs in the

717 reference gff file (**F**) are shown with arrows indicating the direction of transcription. Table of TPMs
718 calculated with Salmon for transcripts and FADU for CDSs (**G**) for the same region shown in panels
719 **ABCDEF**. For ONT reads, only Salmon was used. Plot of the $\log_2(\text{TPM})$ for all CDSs and all corresponding
720 transcripts for ERR393285 (**H**). Heatmap clustered by genes for the $\log_2(\text{TPM})$ for all CDSs calculated with
721 FADU and all corresponding transcripts calculated with Salmon for Illumina and ONT reads generated
722 from LB and DMEM (**I**).

723 **Figure 6 – ONT sequencing characteristics that informed algorithm development**

724 Size distribution of all of the *E. coli* K12 ONT sequencing reads aligning outside the rRNA reads compared
725 to the distribution of predicted operons (**A**). For the 285,619 reads that are longer than the operon they
726 map to, the length of reads is plotted relative to the size of the operon they map to (**B**). Normalized
727 sequencing depth from the 3'-end to the 5'-end for *E. coli* K12 16S rRNA, *E. coli* K12 23S rRNA, and IVT
728 RNA (SRR23886069), all thought to be complete, showing the 3'-bias in sequencing (**C**). Distribution of
729 read lengths for the 1.3 kbp yeast enolase ONT spike-in (**D**) and an 11.7 kbp IVT RNA (**E**) from
730 SRR23886069 where only reads ending at the far right position are shown. The log transformed ratios of
731 Illumina (SRR3111494) and ONT (SRR23886071) TPM values for RNA isolated from adult female *Brugia*
732 *malayi*, a filarial nematode and invertebrate animal, is compared to the transcript length, illustrating
733 how shorter transcripts have more Illumina reads relative to ONT reads than longer transcripts (**F**). Our
734 interpretation is that ONT sequencing is biased toward shorter transcripts. The inset uses the heat
735 function to show the intensity of the points in the region which contains most of the data.

736 **Additional Files**

737 **Table A1 – Sequencing statistics for ONT direct RNA sequencing runs with *E. coli* RNA**

738 **Table A2 – Data Used in the Analysis and Prediction of Transcripts**

739 **Figure A1 – *recBCD/ptrA* Transcript Predictions**

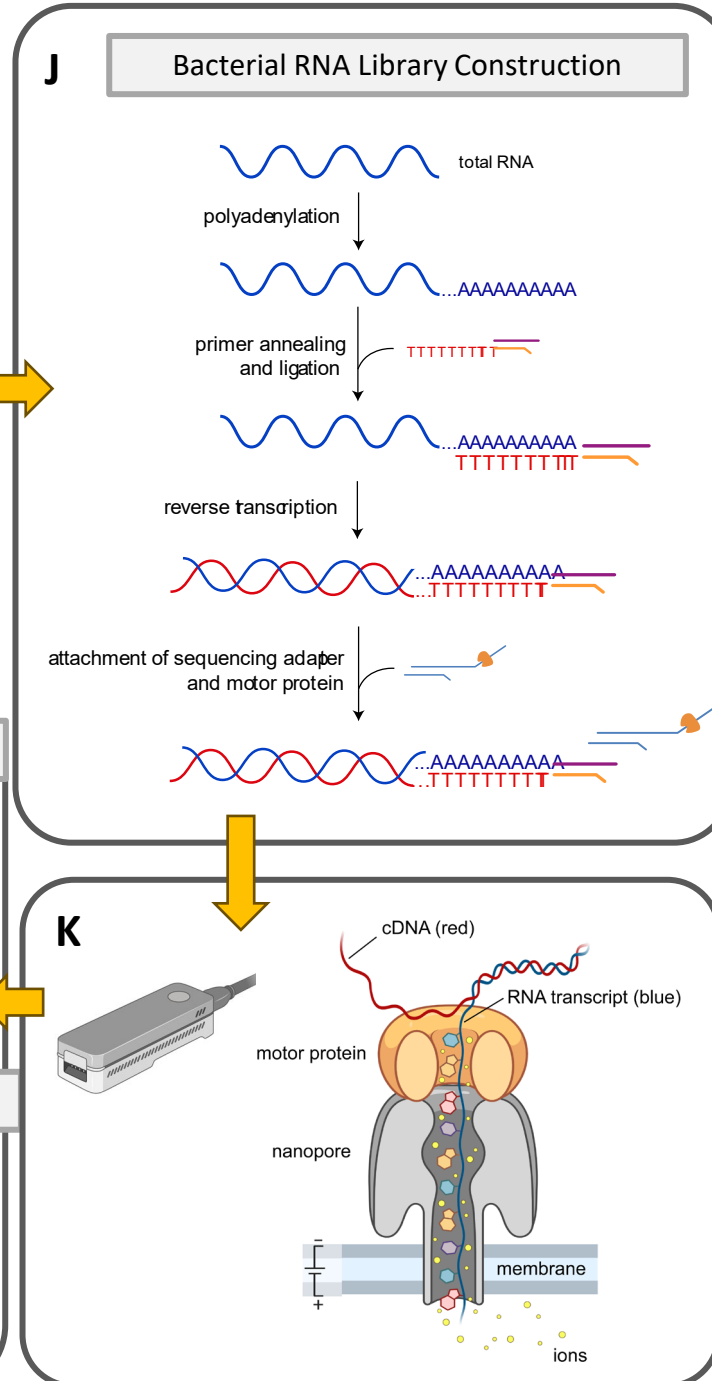
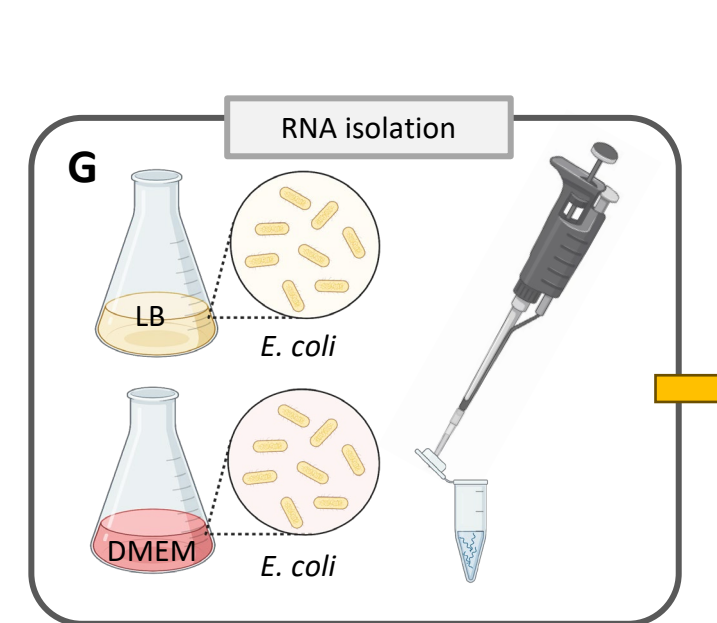
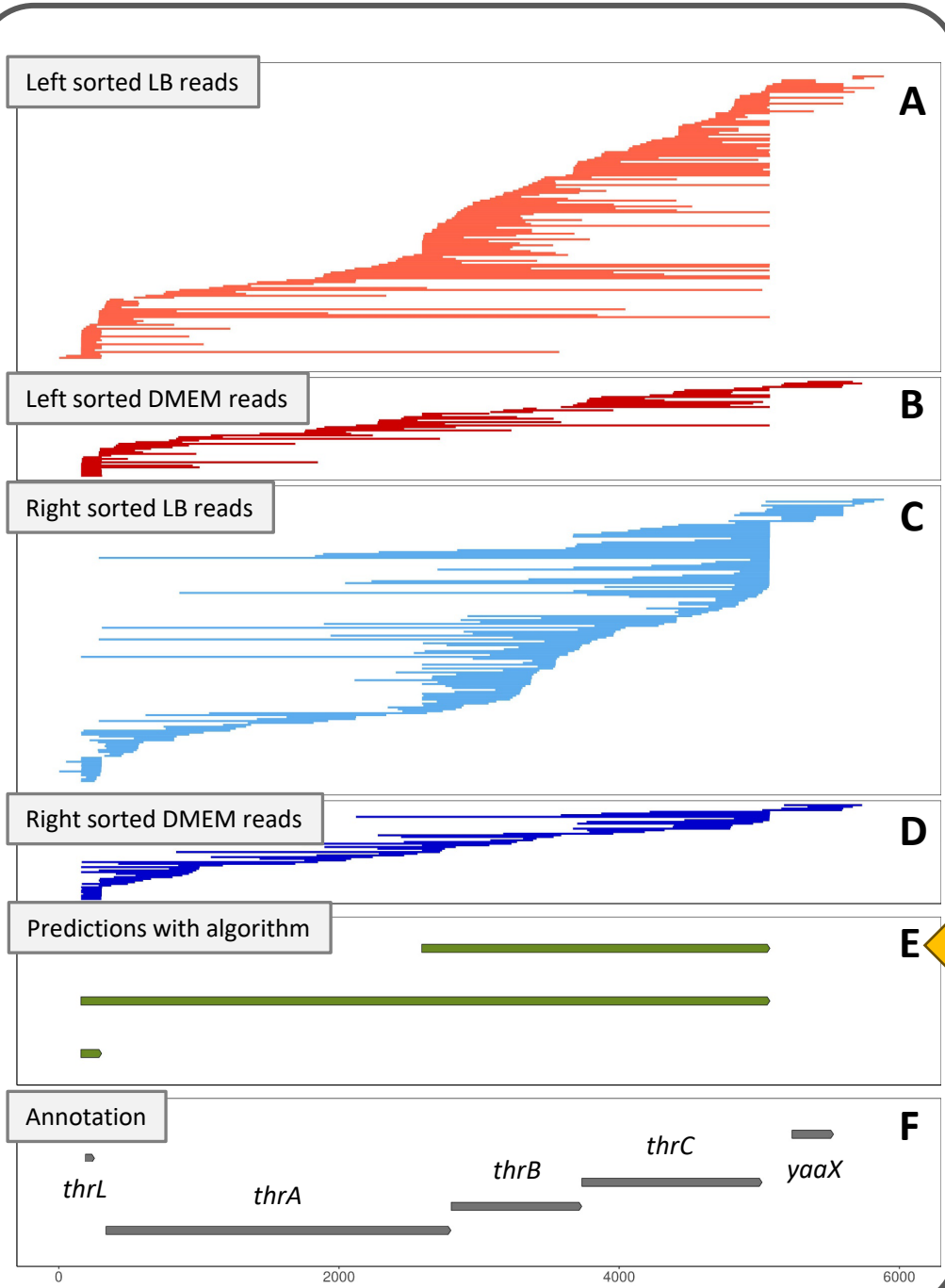
740 Minus-strand ONT direct RNA sequencing reads (shown as lines) are mapped from ~2.950-2.965 Mbp in
741 the *E. coli* K12 genome (NC_000913.3), which corresponds to a region encoding RecBCD and PtrA. Reads
742 are sorted by their transcription stop site for *E. coli* K12 grown in rich LB media (left sorted, **A**; right
743 sorted, **C**) and DMEM media (left sorted, **B**; right sorted, **D**). Our algorithm predicts 3 transcripts (**E**), and
744 7 CDSs in the reference NC_000913.3 GFF file are illustrated (**F**). While there are no ONT reads that span
745 the entire *recBCD/ptrA* region, there is sufficient evidence to call this transcript. This is because, after
746 removing reads wholly contained within a predicted *recBD* transcript and a *ptrA/recBD* transcript there
747 were sufficient reads remaining to predict a transcript that spans *recBCD/ptrA*.

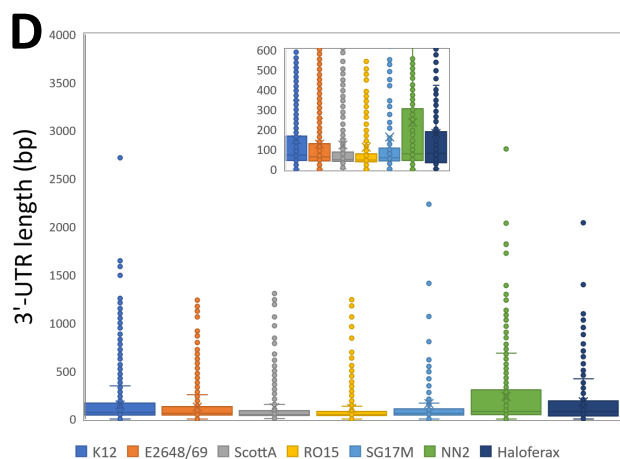
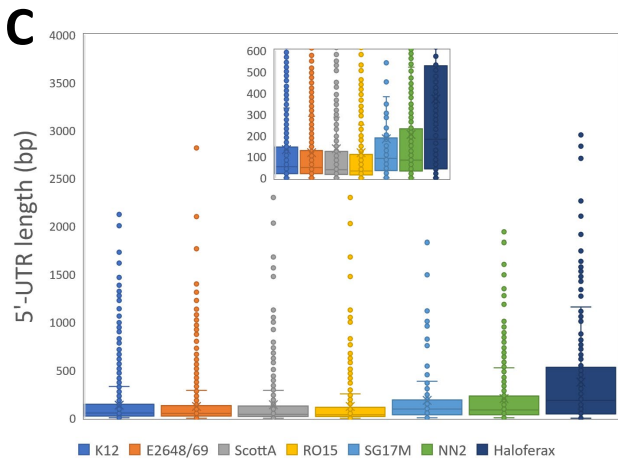
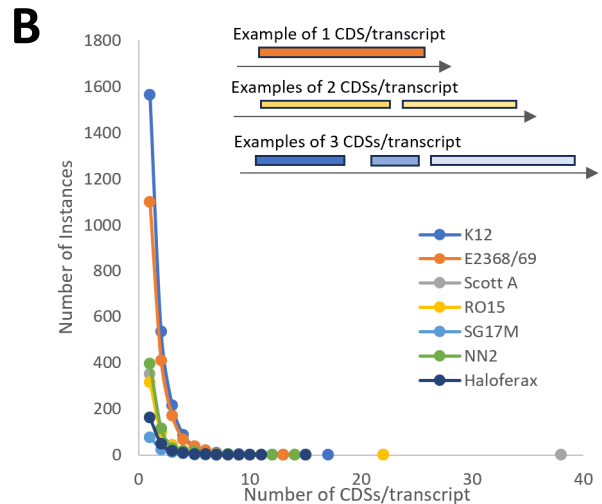
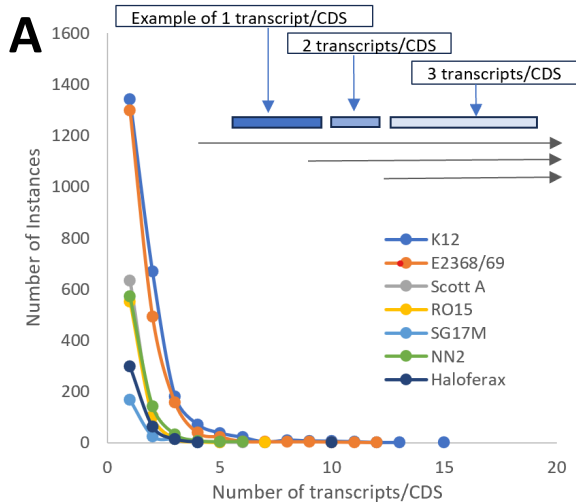
748 **Figure A2 -- Pore-mediated and ligase-mediated chimeras**

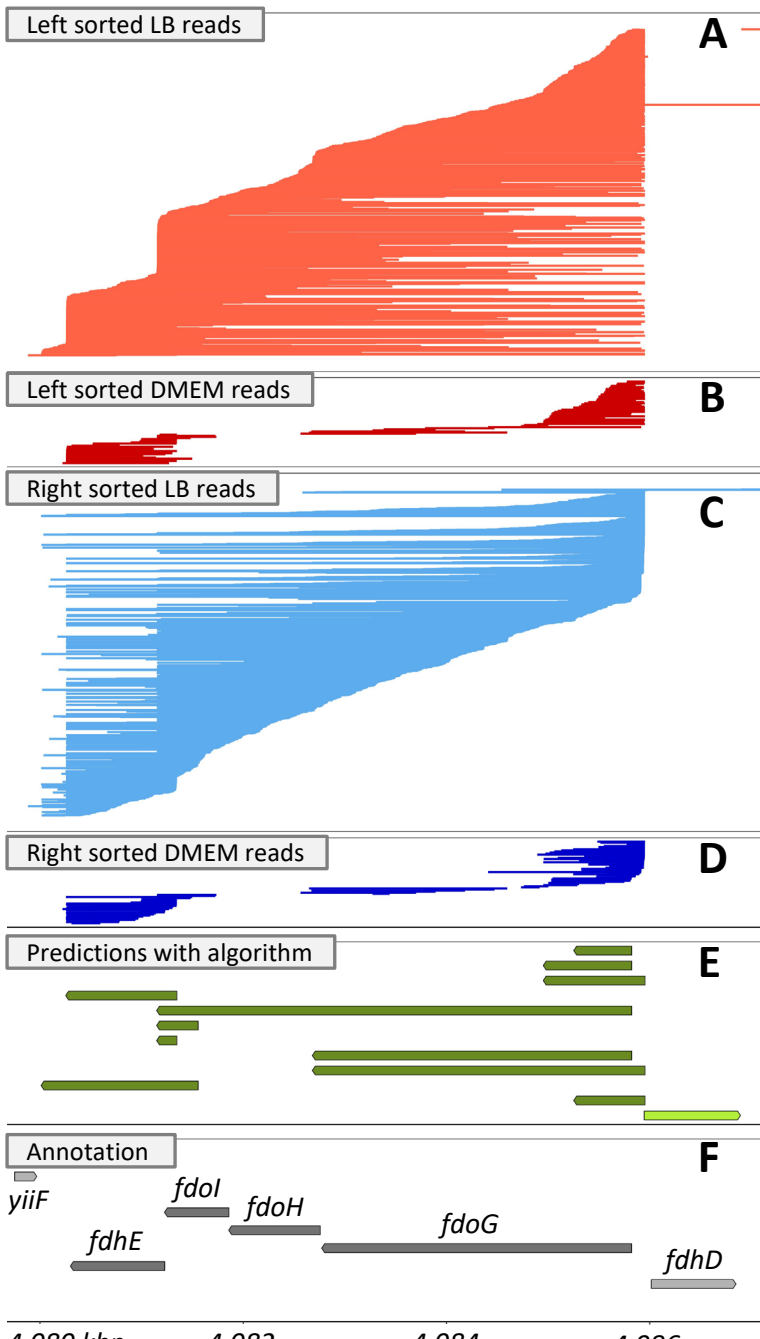
749 Chimeric sequencing reads observed in ONT direct RNA sequencing data can theoretically be generated
750 by (A) two reads entering the pore in tandem with an open pore state that is not detected, (B) two RNA
751 molecules being fused through ligation in vivo, in vitro during library construction, or a mapping artifact
752 when there is a rearrangement in the genome reference, and (C) two fragments fused by ligation
753 following adapter ligation during library construction. (D) A chimeric read from a sequencing run that
754 shows that an open pore state (black) was missed between the first read (blue) and the second read
755 (red). For both reads, the characteristic DNA adaptor with a lower current is observed followed by a
756 higher plateau that is the polyA tail being sequenced. The open pore state is a spike from increased
757 current when the pore is open between RNA molecules sequenced.

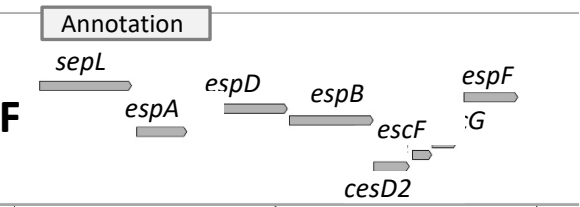
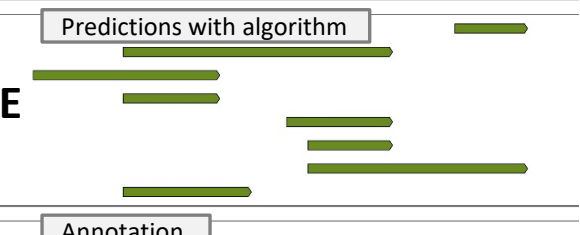
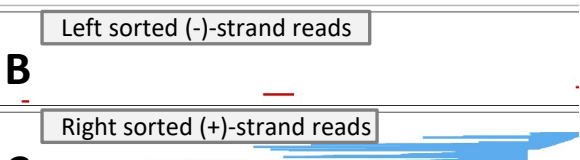
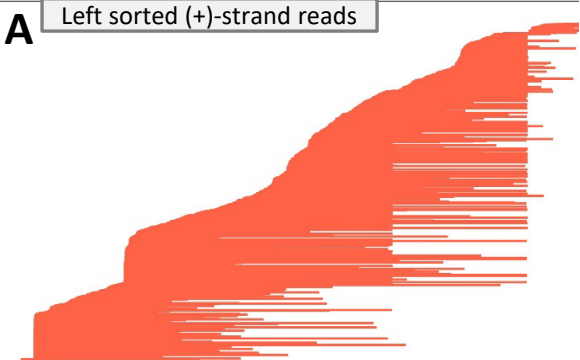
758 **Figure A3 -- Results from Stringtie, Tama, and Cupcake**

759 Transcript predictions resulting from Stringtie, Tama, and Cupcake are shown for *E. coli* K12 for the same
760 region as presented in Figure 3. Plots are labeled on the right side according to the notation in the
761 github page that fully describes how they were run with those ending in LB resulting from only the K12
762 LB data and those ending in DMEM resulting from only the K12 DMEM data. Stringtie is splicing focused,
763 and since bacteria do not have splicing it is unsurprising that it could not predict transcript structures,
764 largely yielding transcript predictions corresponding to zero-depth regions across the genome. Whether
765 default (Tama 1) or user-defined parameters were used (Tama 2 and 3), Tama frequently over-called
766 transcripts, particularly in regions with higher sequencing depth. With default parameters (Cupcake 1),
767 Cupcake tends to under-call transcripts because ONT reads get filtered out of analysis due to higher
768 degree of mismatches, and in this region no results were reported. When the parameters were adjusted
769 to better fit ONT reads (Cupcake 2), Cupcake produced results similar to TAMA.









72000 75000 78000

